

Copyright © 2001, by the author(s).  
All rights reserved.

Permission to make digital or hard copies of all or part of this work for personal or classroom use is granted without fee provided that copies are not made or distributed for profit or commercial advantage and that copies bear this notice and the full citation on the first page. To copy otherwise, to republish, to post on servers or to redistribute to lists, requires prior specific permission.

**EFFECT OF Ar ADDITION TO AN O<sub>2</sub> PLASMA  
IN A LARGE AREA PLASMA SOURCE: O<sub>2</sub>/Ar  
MIXTURE PLASMA MODELING AND  
PHOTORESIST ETCHING**

by

Kazushige Takechi and M. A. Lieberman

Memorandum No. UCB/ERL M01/1

4 January 2001

**EFFECT OF Ar ADDITION TO AN O<sub>2</sub> PLASMA  
IN A LARGE AREA PLASMA SOURCE: O<sub>2</sub>/Ar  
MIXTURE PLASMA MODELING AND  
PHOTORESIST ETCHING**

by

Kazushige Takechi and M. A. Lieberman

Memorandum No. UCB/ERL M01/1

4 January 2001

**ELECTRONICS RESEARCH LABORATORY**

College of Engineering  
University of California, Berkeley  
94720

# **Effect of Ar Addition to an O<sub>2</sub> Plasma in a Large Area Plasma Source: O<sub>2</sub>/Ar Mixture Plasma Modeling and Photoresist Etching**

Kazushige Takechi<sup>1</sup> and M. A. Lieberman<sup>2</sup>

<sup>1</sup>*Visiting Industrial Fellow, NEC Corporation in Japan*

<sup>2</sup>*Department of Electrical Engineering and Computer Sciences*

*University of California at Berkeley*

*Berkeley, CA 94720*

## **ABSTRACT**

We report on the effect of Ar addition to an oxygen plasma on photoresist etching in the LAPS. We also develop a simplified spatially-varying O<sub>2</sub>/Ar mixture discharge model corresponding to the LAPS in a two-dimensional geometry in order to account for the effect of Ar addition. A photoresist etch kinetics model and spatially-varying O<sub>2</sub>/Ar mixture discharge model are used to explain the experimental data. We find that the addition of 50% Ar increases the plasma density and etch rate approximately by a factor of two. From the simulation, we find that argon metastables (Ar\*) play an important role in the mixture plasma. The simulation predicts an enhancement in O-atom density ratio due to Ar addition over that due to the dilution of the feed gas. The experimental data and predicted etch rates from the simulation are generally in good agreement, indicating that the increase in the etch rate with Ar addition is due to both the increase in the plasma density and the enhancement in O-atom density attributable to the dissociation of O<sub>2</sub> by Ar\*.

## **1. Introduction**

For an inductively coupled, traveling wave driven, large area plasma source (LAPS), we have previously developed a simplified spatially-varying oxygen discharge model and photoresist etch kinetics model in order to explain the etch rate behavior dependence on the oxygen gas pressure.<sup>1,2</sup>

Mixtures of reactive and rare gases are often used for thin film etching and deposition in microelectronics fabrication. Several studies have been conducted to determine the effect of adding rare gases to reactive gas plasmas. Bassett *et al.* have developed a Cl<sub>2</sub>/Ar mixture discharge model and have found that argon metastables (Ar\*) can induce the dissociation of chlorine when Ar is added to Cl<sub>2</sub>.<sup>3</sup> Booth *et al.* have observed that the addition of Kr to an O<sub>2</sub> plasma increases the degree of dissociation in their O-atom actinometry experiments.<sup>4</sup>

In this letter, we investigate the effect of Ar addition to an oxygen plasma on photoresist etching in the LAPS. We also describe a simplified spatially-varying O<sub>2</sub>/Ar mixture discharge model corresponding to the LAPS in a simplified two-dimensional geometry in order to account for the effect of Ar addition. Specifically a 50% O<sub>2</sub>-50% Ar discharge is compared to a pure O<sub>2</sub> discharge. The photoresist etch kinetics model and spatially-varying O<sub>2</sub>/Ar mixture discharge model are used to understand the experimental data.

## **2. Experiments**

We measured plasma density profiles along a vertical line (perpendicular to the antenna rods) with a Langmuir probe approximately 5 cm in front of the substrate holder, and identified the achievement of launching a traveling wave using four voltage sensors equally spaced along the antenna coil.

Figure 1 shows O<sub>2</sub>/Ar mixture plasma density profiles for different mixing ratios at a total gas pressure of 20 mTorr and an rf power of 1000 W. We see that the plasma density increases as the Ar fraction increases. The addition of 50% Ar increases the plasma density by a factor of 2. In a noble gas like Ar, the collisional energy loss per electron-ion pair created can be lower than for a molecular gas like O<sub>2</sub> at the same electron temperature, resulting in the higher plasma density.<sup>5</sup>

For the measurements of photoresist etch rate, half of a four-inch silicon wafer with 2 μm of hardbaked Novolak photoresist was clamped at the center of the processing area. Typical operating parameters were a total gas pressure of between 1 and 50 mTorr and an rf source power of 1000 W.

Figure 2 shows the dependence of the etch rate on the Ar fraction for a total gas pressure of 20 mTorr. Upon adding 50% of Ar the etch rate is increased approximately by a factor of two and further addition of Ar decreases the etch rate.

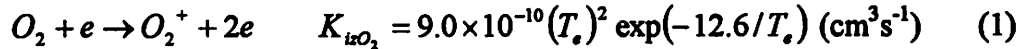
Figure 3 shows the etch rate as a function of both gas pressure and substrate bias voltage ( $V_{\text{bias}}$ ), for a pure  $O_2$  plasma (solid symbols) and an  $O_2/Ar$  mixture with 50%  $O_2$ -50%  $Ar$  (open symbols). The effect of applying a substrate bias on photoresist etching has been previously reported.<sup>2</sup> We see that the addition of 50%  $Ar$  increases the etch rate for gas pressures of 1, 5, 20, and 50 mTorr. If the O-atom density were proportional to  $O_2$  partial pressure, we would not see such an etch rate behavior. In order to explain the etch rate data in Fig. 3, a simplified  $O_2/Ar$  mixture discharge model are introduced in the next section.

### 3. $O_2/Ar$ mixture discharge model

The  $O_2/Ar$  mixture discharge model we will describe below is similar to the previously developed oxygen discharge model,<sup>1</sup> except that reactions for  $Ar$  and  $Ar^*$  are included. For  $Ar^*$  loss processes, we include the collisional de-excitation with electrons and the dissociation of  $O_2$  by  $Ar^*$ . We also include wall quenching, in which  $Ar^*$  is de-excited upon striking the chamber walls.

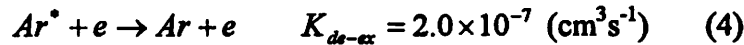
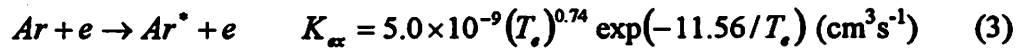
Assumptions of our model are listed below.

- (1) Steady state is assumed.
- (2) For simplicity, we ignore negative ions. We thus take  $n = n_i = n_e$ , where  $n$  is the plasma density,  $n_i$  is the positive ion density, and  $n_e$  is the electron density.
- (3) The mixing ratio of  $O_2/Ar = 1/1$  is assumed.
- (4) We take into account the following two reactions for the ionization process.<sup>5,6</sup>



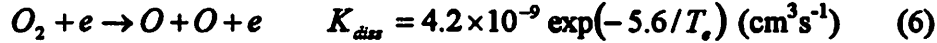
where  $K_{izO_2}$  is the molecular oxygen ionization rate constant and  $K_{izAr}$  is the argon ionization rate constant.

- (5) The following reactions for  $Ar$  and  $Ar^*$  are included.<sup>7,8</sup>



$K_{diss^*}$  has been estimated from similar reactions in  $Cl_2/Ar$  and  $F_2/Ar$  mixtures.<sup>3,7</sup> By assuming  $K_{diss^*}$  is inversely proportional to the molecular bond strength, with  $K_{diss^*}=4.7 \times 10^{-10} \text{ cm}^3\text{s}^{-1}$  for  $Cl_2$  with bond strength 250 kJ/mol, and with  $K_{diss^*}=6.2 \times 10^{-10} \text{ cm}^3\text{s}^{-1}$  for  $F_2$  with bond strength 160 kJ/mol, we obtain for  $O_2$  with bond strength 490 kJ/mol that  $K_{diss^*}=2.4 \times 10^{-10} \text{ cm}^3\text{s}^{-1}$ .

(6) In addition to reaction (5), the following reaction is included for the oxygen dissociation.<sup>5,6</sup>



(7) The ion loss velocity is the Bohm velocity  $u_B = (eT_e/M_{Av})^{1/2}$ , where  $M_{Av}$  is the average ion mass.

(8) The ion temperature  $T_i$  and neutral species temperature  $T_n$  are assumed to be 0.05 V for gas pressures ranging from 1 mTorr to 100 mTorr.

Solving Eq. (7) as an eigenvalue problem with the proper boundary conditions gives the plasma density profile and the electron temperature:

$$\nabla^2 n(x, y) + n(x, y) \frac{K_{izAr} n_{Ar} + K_{izO_2} n_{O_2}}{D_a} \sum_{i=1}^8 \exp\left(\frac{R - r_i(x, y)}{\lambda_{iz-Av}}\right) = 0 \quad (7)$$

where  $n(x, y) = n_i(x, y) = n_e(x, y)$  is the plasma density profile and  $D_a = (T_e/T_i)^{1/2} u_B / (n_{O_2} + n_{Ar}) \sigma_i$  is the ambipolar diffusion coefficient, with  $u_B = (2eT_e / (M_{Ar} + M_{O_2}))^{1/2}$  the mean Bohm velocity,  $\sigma_i = 10^{-14} \text{ cm}^2$  the ion-neutral cross section, and  $n_{O_2}$  and  $n_{Ar}$  the gas densities. We incorporate an exponentially decreasing electron-neutral ionization around each quartz tube, where  $R$  is the radius of the quartz tubes,  $r_i(x, y)$  is the distance from the center of each quartz tube, and  $\lambda_{iz-Av}$  is the average electron-neutral ionization length. For the mixture of  $O_2/Ar = 1/1$ , we use the following expression for the ionization length:

$$\lambda_{iz-Av} = \frac{\lambda_{iz(Ar)} + \lambda_{iz(O_2)}}{2} = \frac{125}{p(\text{mTorr})} + \frac{80}{p(\text{mTorr})} \text{ (cm)}, \quad (8)$$

which is consistent with previous expression used for argon and oxygen discharges.<sup>1,9</sup>

Using the obtained electron temperature  $T_e$  and plasma density profile  $n(x, y)$ , we solve a diffusion equation (9) to determine the  $Ar^*$  density profile:

$$-D_{Ar^*} \nabla^2 n_{Ar^*}(x, y) = K_{ex} n_{Ar} n(x, y) - K_{de-ex} n_{Ar^*}(x, y) n(x, y) - K_{diss^*} n_{Ar^*}(x, y) n_{O_2} \quad (9)$$

with the following boundary condition (10):

$$-D_{Ar^*} \nabla n_{Ar^*}(x, y) |_{walls} = \frac{1}{4} n_{Ar^*}(x, y) \overline{v_{O_2-Ar, Ar^*}}, \quad (10)$$

where  $D_{Ar^*} = \frac{\pi}{8} \frac{1}{(n_{O_2} + n_{Ar}) \sigma_{O_2-Ar, Ar^*}} \overline{v_{O_2-Ar, Ar^*}}$  is the diffusion coefficient with  $\sigma_{O_2-Ar, Ar^*} = 5 \times 10^{-15} \text{ cm}^2$  the cross section and  $\overline{v_{O_2-Ar, Ar^*}} = 8.2 \times 10^4 \text{ cm/s}$  the mean speed.

Using the obtained plasma density profile  $n(x, y)$  and  $Ar^*$  density profile  $n_{Ar^*}(x, y)$ , we solve another diffusion equation (11) to determine the O-atom density profile  $n_O(x, y)$ :

$$-D_O \nabla^2 n_O(x, y) = 2K_{\text{dis}} n(x, y) n_{O_2} + 2K_{\text{dis}^*} n_{Ar^*}(x, y) n_{O_2}, \quad (11)$$

with the same expression for  $D_O$  and boundary conditions as in the previous work,<sup>1</sup> in which the metal-surface recombination coefficient  $\gamma_{\text{metal}}$  is assumed to be 0.1 and quartz-surface recombination coefficient  $\gamma_{\text{quartz}}$  is assumed to be 0.0001.

The overall discharge energy balance can be expressed as

$$P_{\text{abs}} = e \oint_{\text{walls}} E_T \Gamma_i dS, \quad (12)$$

where  $P_{\text{abs}}$  is the power absorbed by the plasma,  $E_T$  is the total energy loss,  $dS$  is the area element for particle loss, and  $\Gamma_i$  is the ion flux to the wall surfaces.  $E_T$  is the sum of the collisional energy loss per electron-ion pair created and kinetic energy carried to the walls by electrons and ions.<sup>5</sup> After the density profiles are computed from Eqs. (7), (9), and (11), Eq. (12) is solved to determine the absolute magnitude of the densities in the system.

#### 4. Discussion

We first describe how the computed plasma density and  $T_e$  change depending on the plasma gas composition. Figures 4(a), (b), and (c) show the computed plasma density profiles for a pure Ar, O<sub>2</sub>/Ar mixture, and pure O<sub>2</sub> discharges, respectively, at a gas pressure of 20 mTorr. The corresponding electron temperature is also shown in the figures. For the pure Ar plasma, Eq. (7) was solved with  $n_{O_2}=0$ . For the pure O<sub>2</sub> plasma, Eq. (7) was solved with  $n_{Ar}=0$ . As seen in these figures, the variation of plasma density is similar to the experimental result in Fig. 1, with the plasma density increasing with increasing the Ar fraction. We also see that  $T_e$  decreases with increasing Ar fraction. This result physically means  $K_{\text{izAr}} / D_{a(\text{Ar})} > K_{\text{izO}_2} / D_{a(\text{O}_2)}$  for the  $T_e$  with zero Ar fraction, where  $D_{a(\text{Ar})}$  and  $D_{a(\text{O}_2)}$  are the ambipolar diffusion coefficients for the pure Ar and O<sub>2</sub> plasmas.

Figures 5(a) and (b) show the computed Ar\* density profiles for a pure Ar plasma and an O<sub>2</sub>/Ar mixture with 50% O<sub>2</sub>-50% Ar, respectively, at a total gas pressure of 20 mTorr. The Ar\* density for the pure Ar plasma is higher by a factor of 50 compared to that for the mixture. The same trend has been observed for a Cl<sub>2</sub>/Ar discharge simulation<sup>3</sup> and laser-induced fluorescence (LIF) measurement,<sup>10</sup> in which the Ar\* density was estimated to be  $\sim 10^{11}$  cm<sup>-3</sup> for pure Ar and a drop in the LIF intensity by an order of magnitude was observed for the Cl<sub>2</sub>/Ar mixture. Figure 5(c) shows the computed Ar\* density profiles for an O<sub>2</sub>/Ar mixture with 50% O<sub>2</sub>-50% Ar at a total gas pressure of 5 mTorr. Comparing Fig. 5(b) and 5(c), the Ar\* density is higher at the lower gas pressure. The similar trend has been observed for a Cl<sub>2</sub>/Ar discharge simulation<sup>3</sup>. For the pure Ar plasma, the primary loss mechanisms of Ar\* are

collisions with electrons and wall quenching, while for the mixture it is collisions with O<sub>2</sub>.

Figure 6 shows the dependence of computed T<sub>e</sub> on total gas pressure for a pure O<sub>2</sub> plasma and an O<sub>2</sub>/Ar mixture with 50% O<sub>2</sub>-50% Ar. The trends are similar, with T<sub>e</sub> decreasing with increase pressure.

Figures 7(a) and (b) show the computed O-atom density profiles for a pure O<sub>2</sub> plasma and an O<sub>2</sub>/Ar mixture with 50% O<sub>2</sub>-50% Ar, respectively, at a gas pressure of 20 mTorr. From Eq. (11) with the results in Figs. 4(b), (c), and 5(b), the predicted O-atom density ratio for 20 mTorr scales as

$$\frac{n_o(O_2/Ar)}{n_o(O_2)} \approx \frac{2K_{diss}(O_2/Ar)n(O_2/Ar)n_{O_2}(O_2/Ar) + 2K_{diss}n_{Ar^*}n_{O_2}}{2K_{diss}(O_2)n(O_2)n_{O_2}(O_2)} \approx 0.6,$$

which is in good agreement with the ratio seen in Figs. 7 (a) and (b). Figures 8(a) and (b) show the computed O-atom density profiles for a pure O<sub>2</sub> plasma and the mixture, respectively, at a gas pressure of 5 mTorr. The O-atom density ratio for 5 mTorr is estimated to be ~0.8, which is larger than that for 20 mTorr. The larger enhancement in O-atom density ratio for 5 mTorr due to Ar addition over that due to the dilution of the feed gas can be attributed to the changes in the Ar\* density and the electron temperature, which in turn affect the generation and loss for the O atoms.

Figure 9 shows the computed ion flux to the substrate surface ( $\Gamma_{i-sub}$ ) at various gas pressures for the pure O<sub>2</sub> plasma and the mixture. We see that  $\Gamma_{i-sub}$  is higher for the mixture than the pure O<sub>2</sub> plasma, which is consistent with the results in Figs. 4(b) and (c).

Figure 10 shows the computed O-atom density at the substrate surface ( $n_{O-sub}$ ) at various gas pressures for the pure O<sub>2</sub> plasma and the mixture. As the total gas pressure decreases, the difference in  $n_{O-sub}$  between the pure O<sub>2</sub> plasma and the mixture becomes small, which is consistent with the results in Figs. 7 and 8.

Using the simulation results in Figs. 9 and 10, we predict the photoresist etch rate based on a previously developed expression (13):<sup>2</sup>

$$\frac{n_{O-sub}}{E} \frac{\Gamma_{i-sub}}{1.93 \times 10^{15}} = \frac{n_{O-sub}}{7.05 \times 10^{13}} 1.89 \times 10^{-2} \frac{\eta_{ref}}{\eta} + \frac{\Gamma_{i-sub}}{1.93 \times 10^{15}} 1.72 \times 10^{-3}, \quad (13)$$

where  $\eta_{ref}/\eta$  is the relative etch yield depending on substrate bias voltage. Figure 11 illustrates the etch rate data as a function of both gas pressure and substrate bias voltage ( $V_{bias}$ ), for the O<sub>2</sub>/Ar mixture with 50% O<sub>2</sub>-50% Ar, and the predicted etch rate from Eq. (13) with the simulation results in Figs. 9 and 10. Equation (13) predicts a somewhat lower etch rate than the experimental data for  $V_{bias}=0$  V, but does predict the general trend, with the etch rate increasing with Ar addition as seen in Fig. 3. If we solve only Eq. (7) and Eq. (11) without the second term on the right-hand side, ignoring the Ar\* contribution,

then the predicted etch rates becomes still lower than those in Fig. 11. The increase in the etch rate with Ar addition is, therefore, due to not only the increase in  $\Gamma_{i-sub}$  but also the enhancement in  $n_{O-sub}$  attributable to dissociation of O<sub>2</sub> by Ar\*. Ar\* has a relatively high energy and also a long lifetime because its transition to the ground state is forbidden. Consequently, Ar\* can influence actively the plasma chemistry and therefore the etch processing.

## **5. Conclusions**

The effect of Ar addition to an O<sub>2</sub> plasma on photoresist etching has been investigated in the LAPS. We have also developed a simplified spatially-varying O<sub>2</sub>/Ar (O<sub>2</sub> : Ar = 1 : 1) mixture discharge model corresponding to the LAPS in a two-dimensional geometry in order to account for the effect of Ar addition.

The mixture plasma density increases as the Ar fraction increases. The addition of 50% Ar increases the plasma density by a factor of two. The addition of Ar increases the etch rate for gas pressures of 1, 5, 20, and 50 mTorr. Particularly, for  $V_{bias}=0$  V, the etch rate is approximately doubled by the addition of 50% Ar. From the simulation results, we have found that argon metastables (Ar\*) play an important role in the mixture plasma. The simulation predicts an enhancement in O-atom density ratio due to Ar addition over that due to the dilution of the feed gas depending on the total gas pressure. This can be attributed to the changes in the Ar\* density and the electron temperature. The experimental data and predicted etch rates from the simulation are generally in good agreement, indicating that the increase in the etch rate with Ar addition is due to both the increase in the plasma density and the enhancement in O-atom density attributable to the dissociation of O<sub>2</sub> by Ar\*.

## **References**

- 1) K. Takechi and M. A. Lieberman, J. Appl. Phys. 89, 869 (2001).
- 2) K. Takechi and M. A. Lieberman, Effect of ion energy on photoresist etching in an inductively coupled large area plasma source (LAPS), Memorandum UCB/ERL M00/58, Electronics Research Laboratory, University of California, Berkeley, (2000).
- 3) N. L. Bassett and D. J. Economou, J. Appl. Phys. 75, 1931 (1994).
- 4) J. P. Booth, O. Joubert, and J. Pelletier, J. Appl. Phys. 69, 618 (1991).
- 5) M. A. Lieberman and A. J. Lichtenberg, *Principles of Plasma Discharges and Materials Processing*, John Wiley & Sons Inc., 605 Third Avenue, New York, NY, (1994).
- 6) C. Lee and M. A. Lieberman, J. Vac. Sci. Technol. A 13, 368 (1995).
- 7) F. Kannari, M. Obara, and T. Fujioka, J. Appl. Phys. 57, 1309 (1985).

- 8) S. Ashida, C. Lee, and M. A. Lieberman, *J. Vac. Sci. Technol. A* 13, 2498 (1995).
- 9) V. P. Gopinath and M. A. Lieberman, Simulation and analysis of a large area plasma source, Memorandum UCB/ERL M95/65, Electronics Research Laboratory, University of California, Berkeley, (1995).
- 10) G R. Scheller, R. A. Gottscho, T. Intrator, and D. B. Graves, *J. Appl. Phys.* 64, 598 (1988).

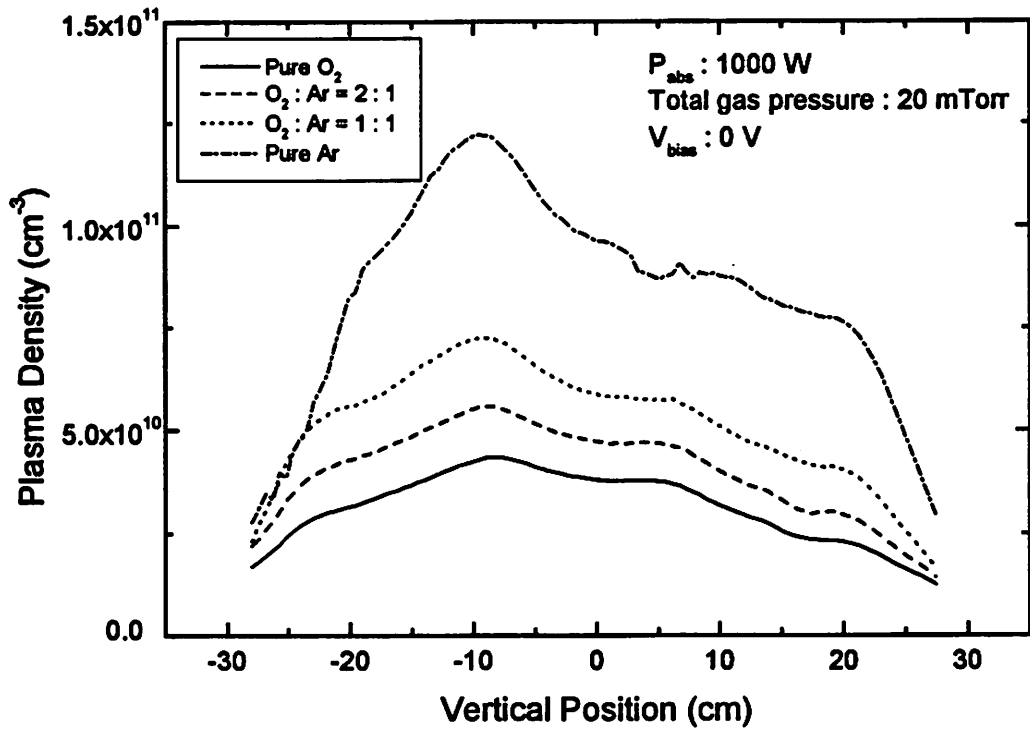


Fig. 1. O<sub>2</sub>/Ar mixture plasma density profiles for different mixing ratios.

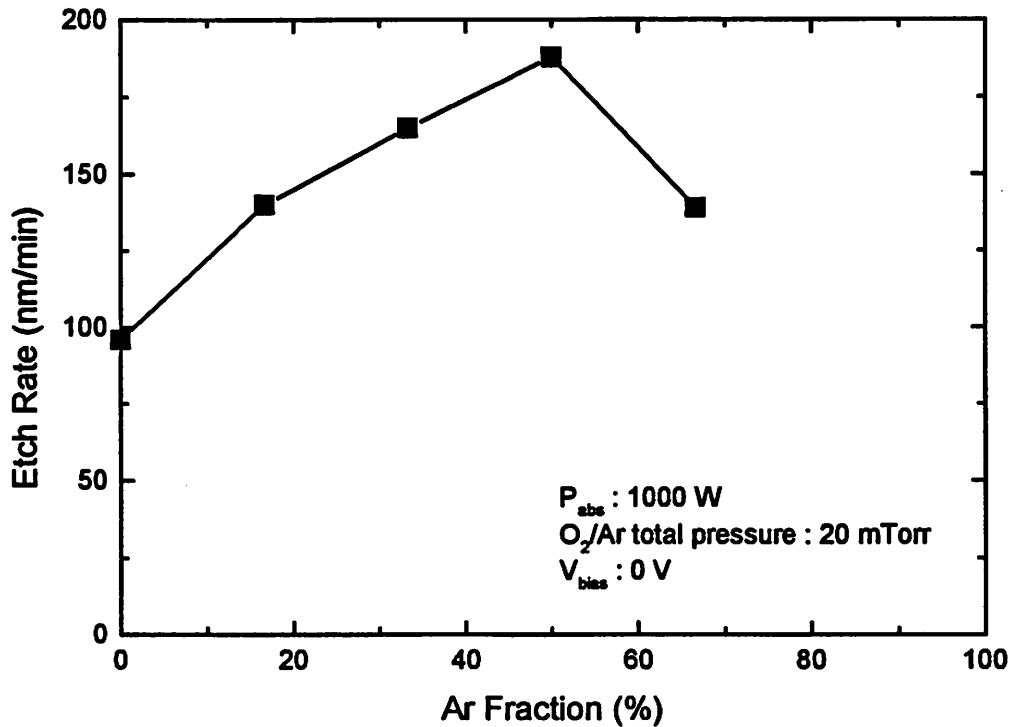


Fig. 2. Dependence of the etch rate on Ar fraction for a total gas pressure of 20 mTorr.

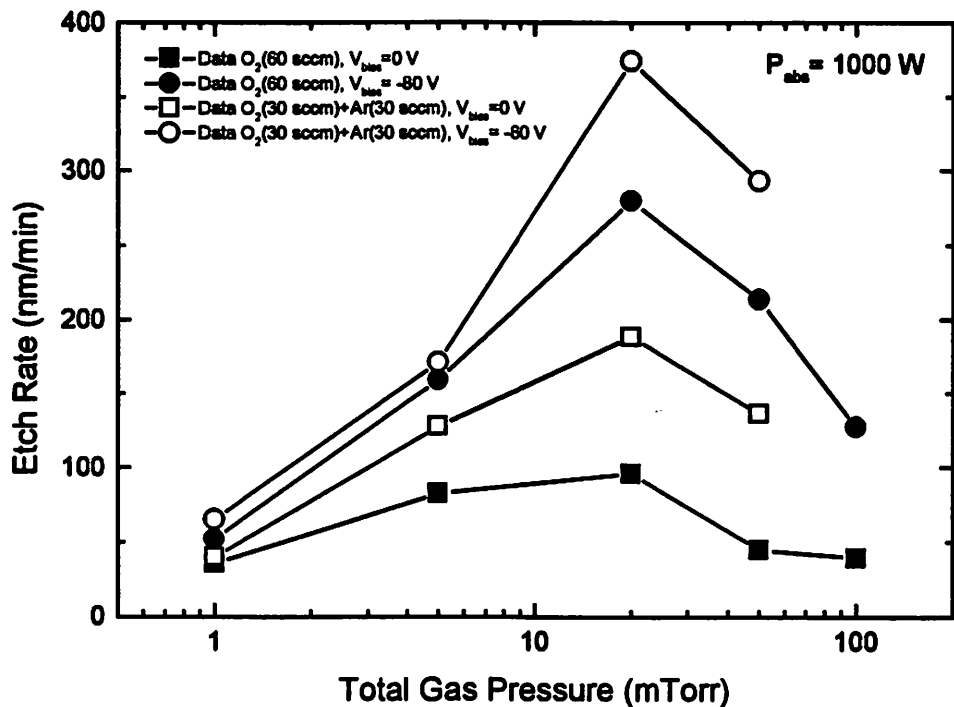


Fig. 3. Etch rate as a function of gas pressure for a pure O<sub>2</sub> plasma and O<sub>2</sub>/Ar mixture with 50% O<sub>2</sub>-50% Ar.

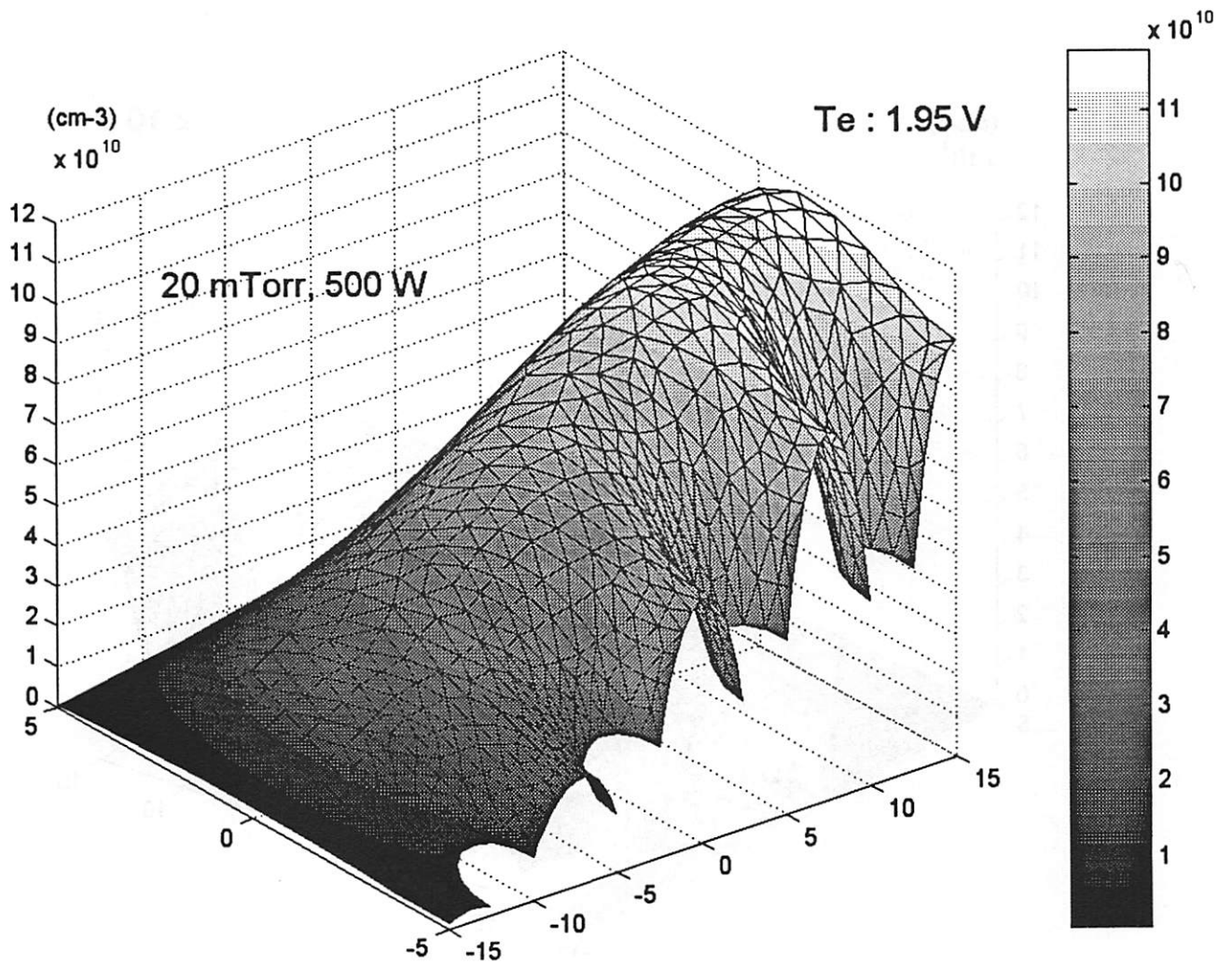


Fig. 4(a). Plasma density profile for a pure Ar discharge.

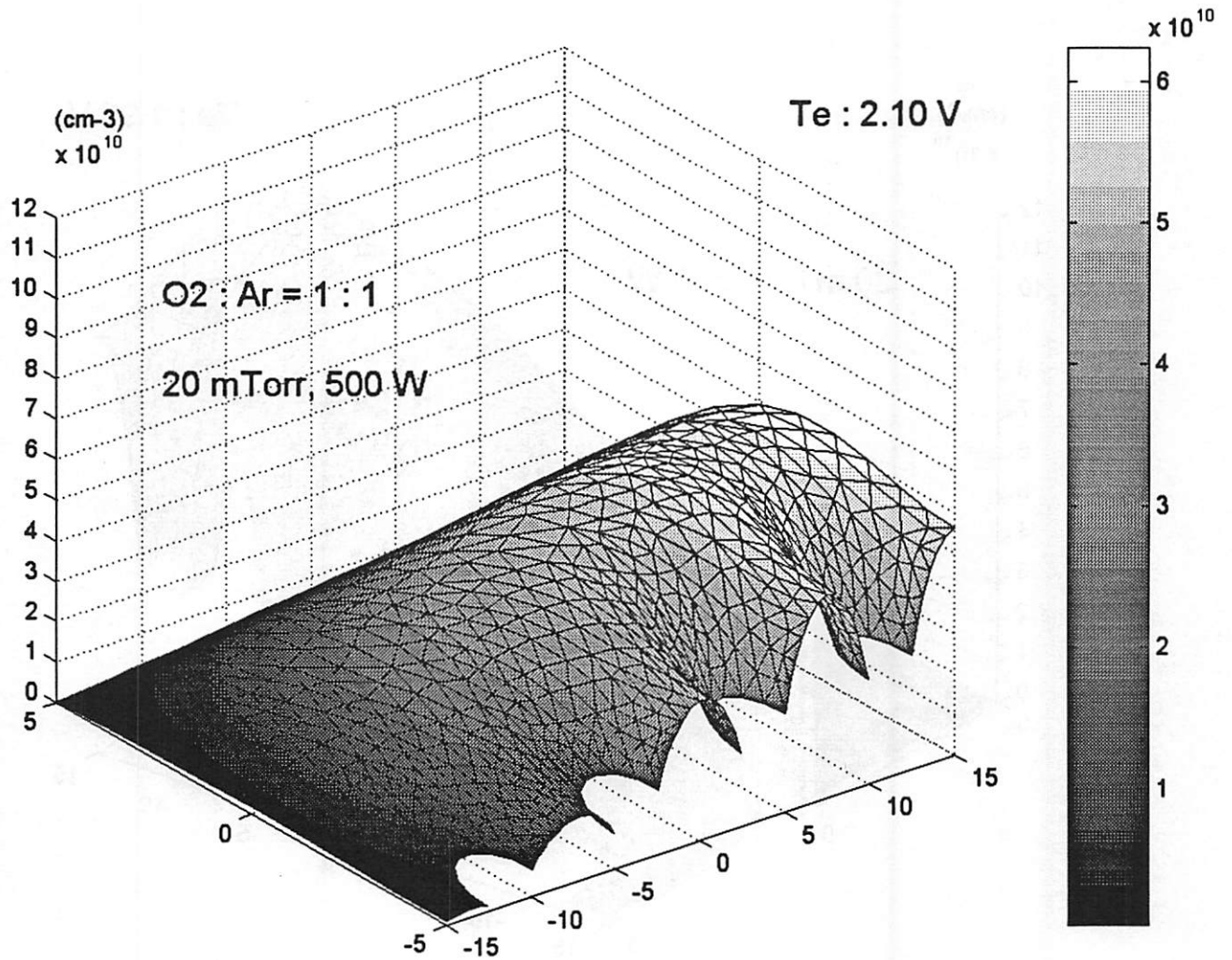


Fig. 4(b). Plasma density profile for an O<sub>2</sub>/Ar mixture discharge.

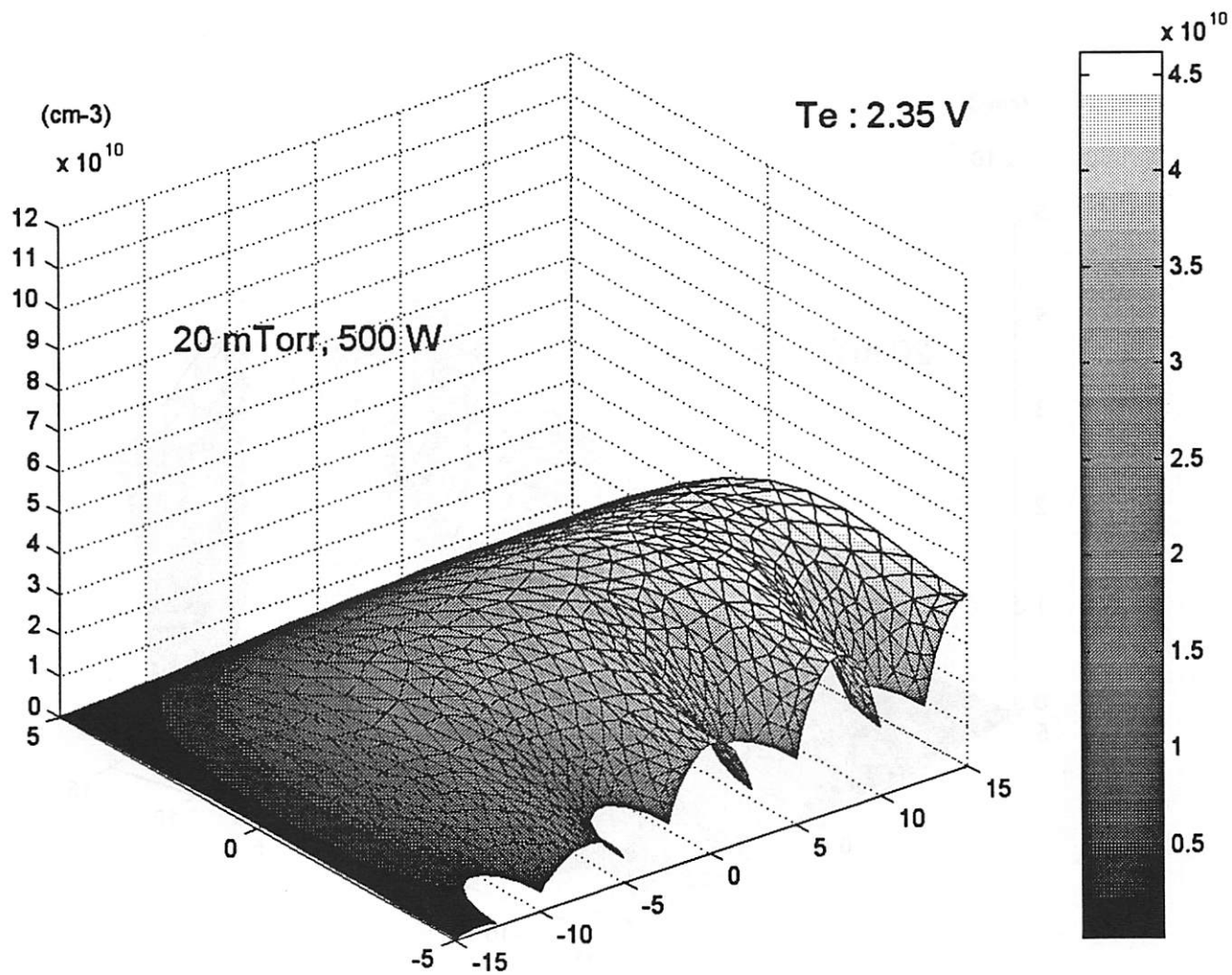


Fig. 4(c). Plasma density profile for a pure O<sub>2</sub> discharge.

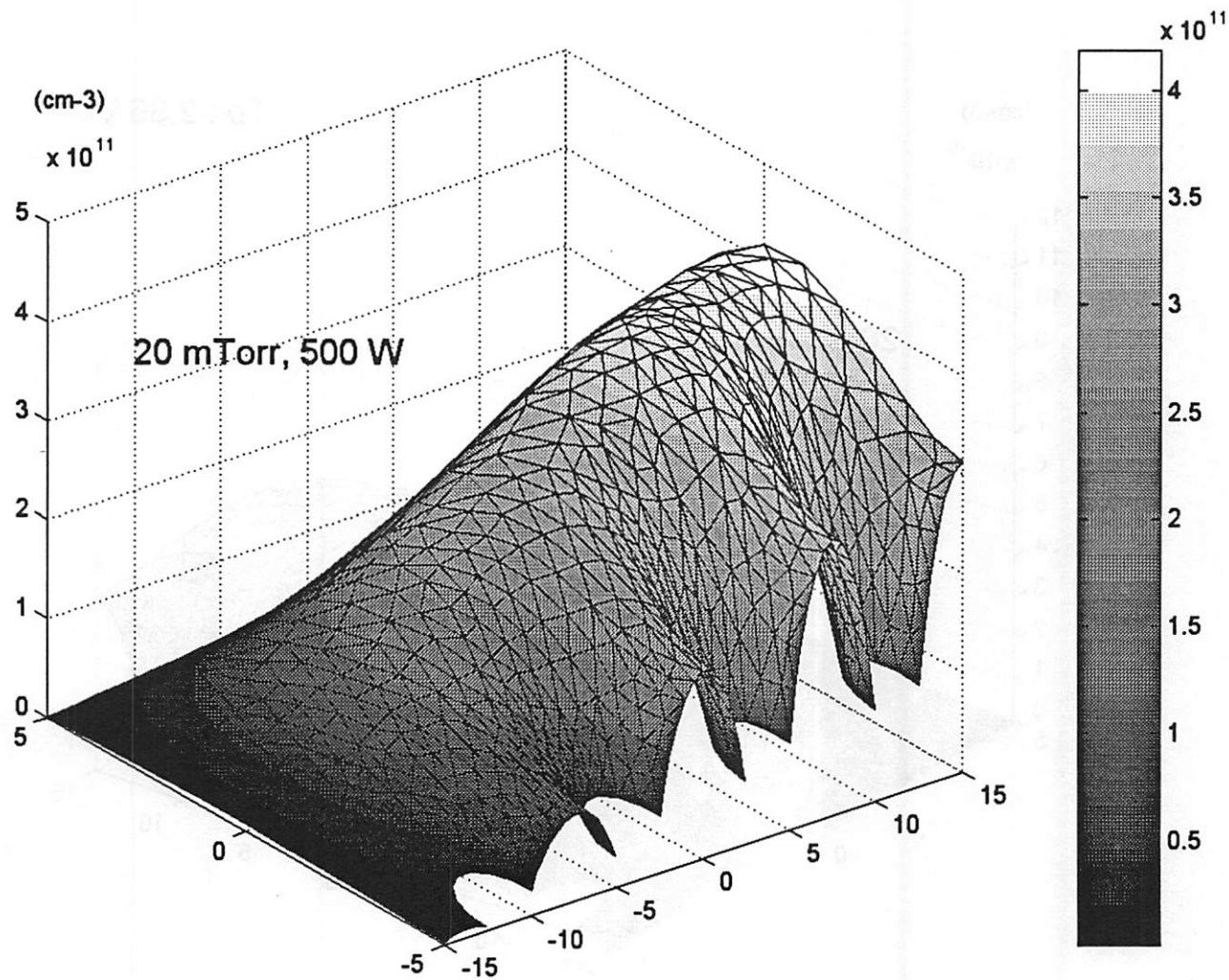


Fig. 5(a). Ar\* density profile for a pure Ar discharge at 20 mTorr.

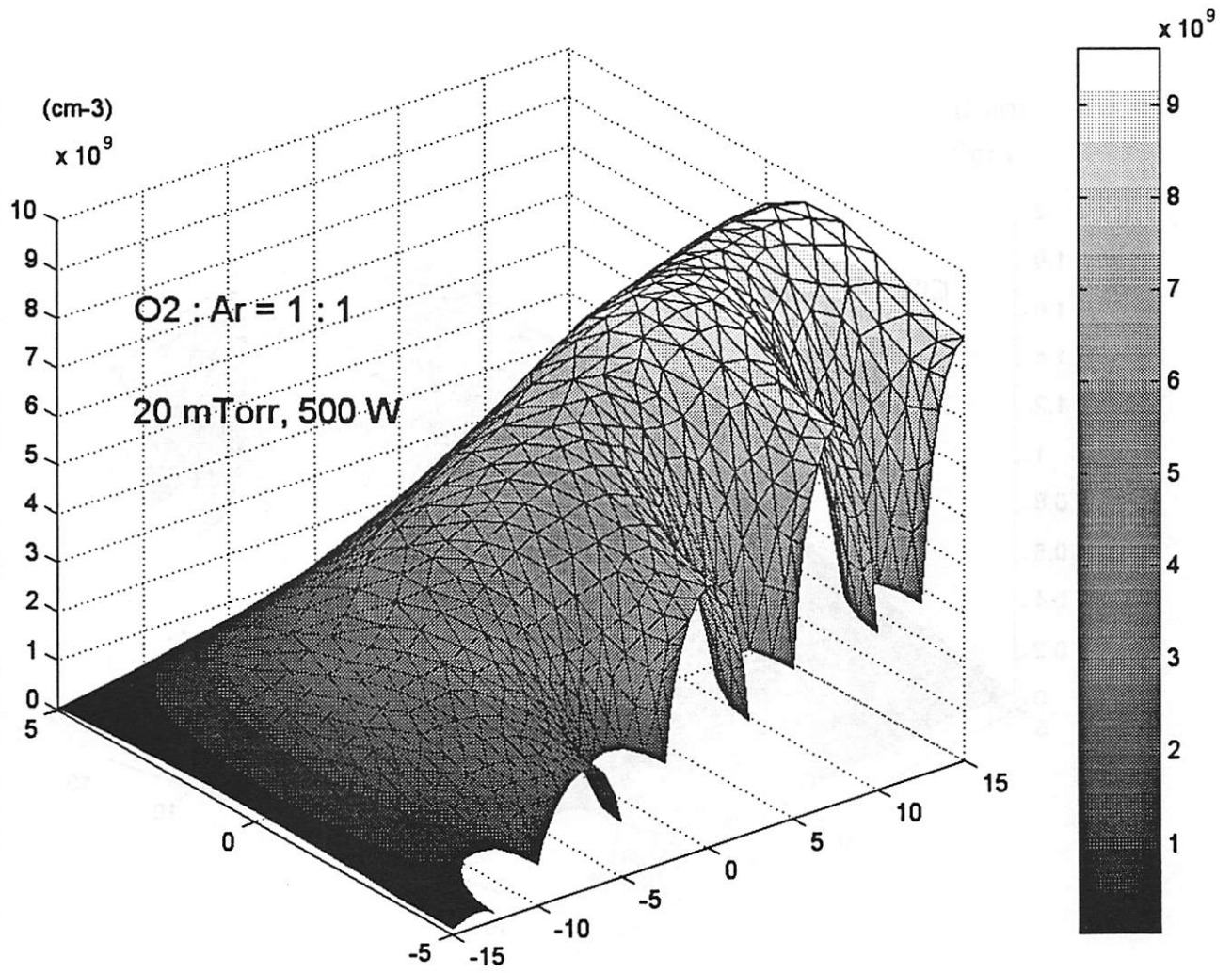


Fig. 5(b). Ar\* density profile for an O<sub>2</sub>/Ar mixture discharge at 20 mTorr.

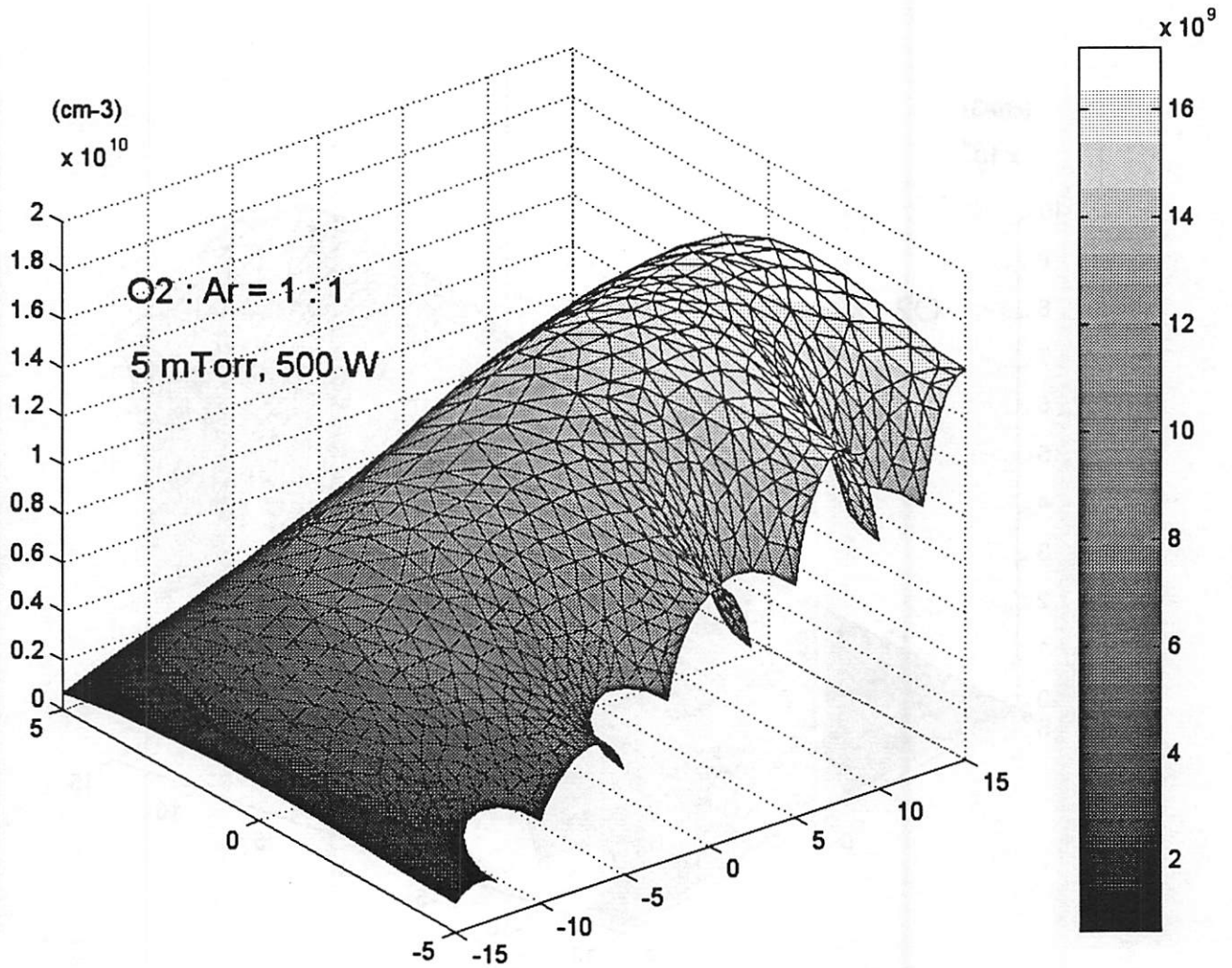


Fig. 5(c). Ar\* density profile for an O<sub>2</sub>/Ar mixture discharge at 5 mTorr.

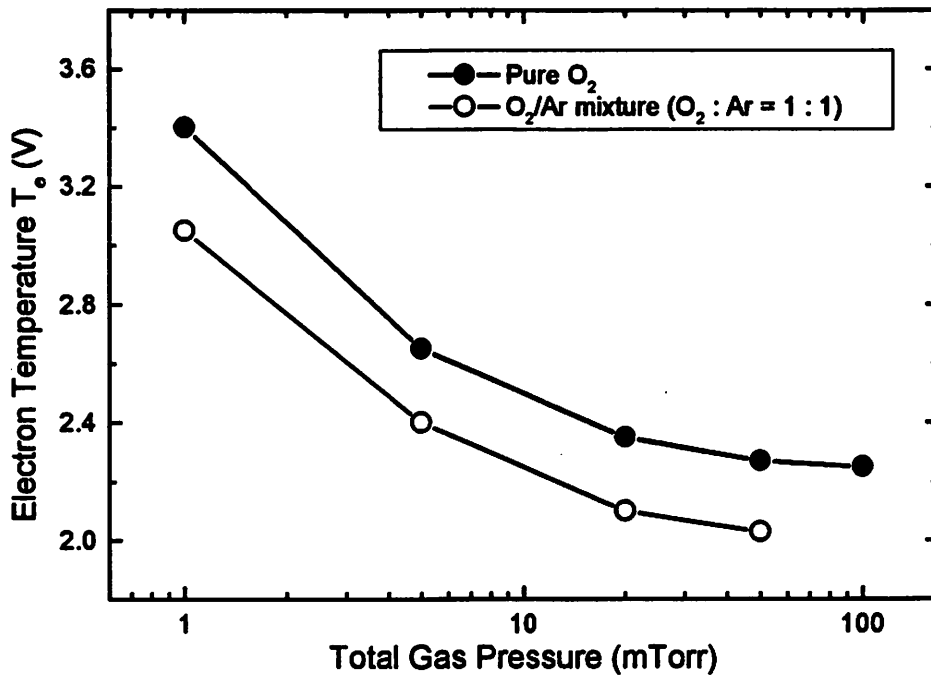


Fig. 6. Dependence of computed  $T_e$  on total gas pressure for a pure O<sub>2</sub> plasma and O<sub>2</sub>/Ar mixture with 50% O<sub>2</sub>-50% Ar.

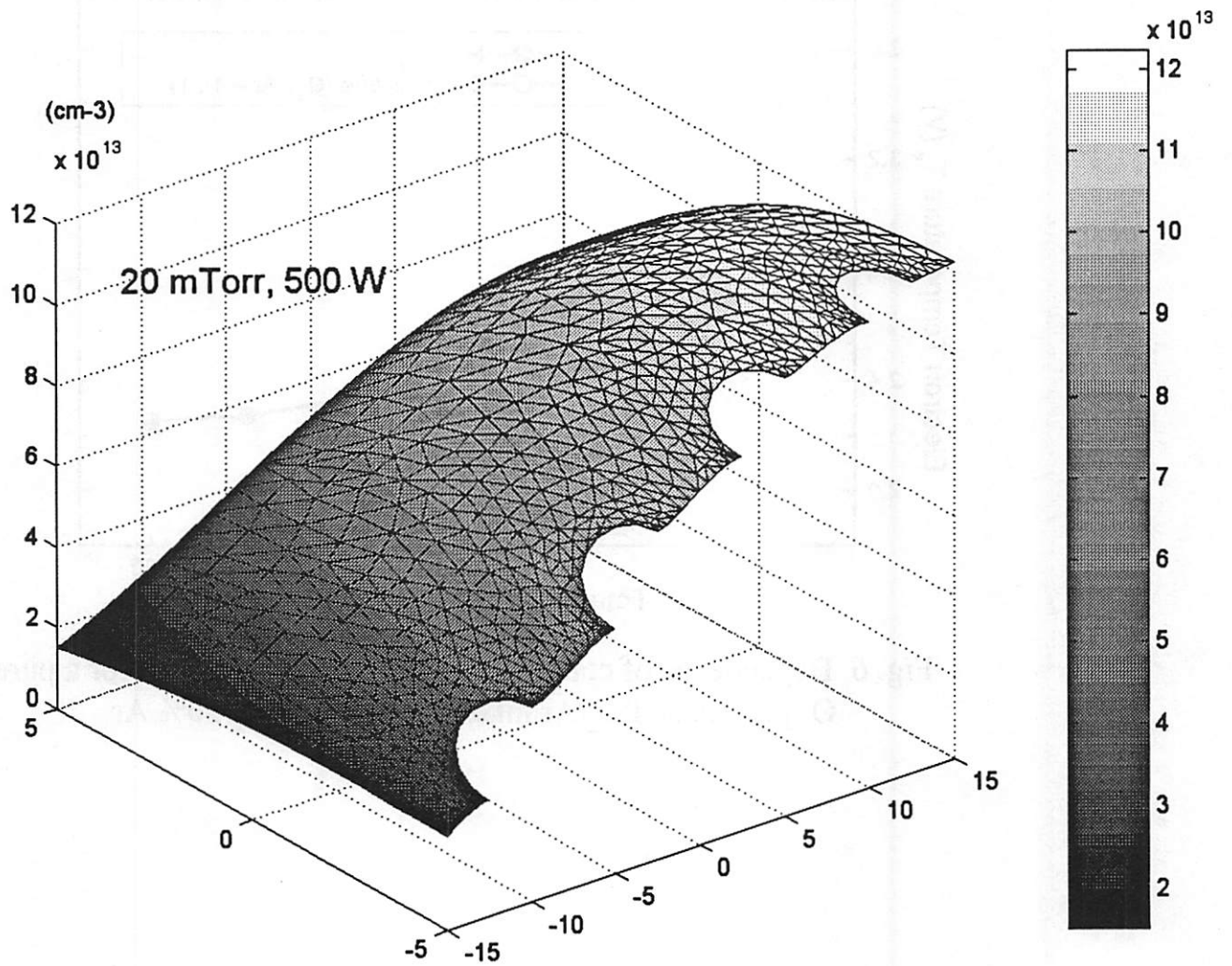


Fig. 7(a). O-atom density profile for a pure O<sub>2</sub> discharge at 20 mTorr.

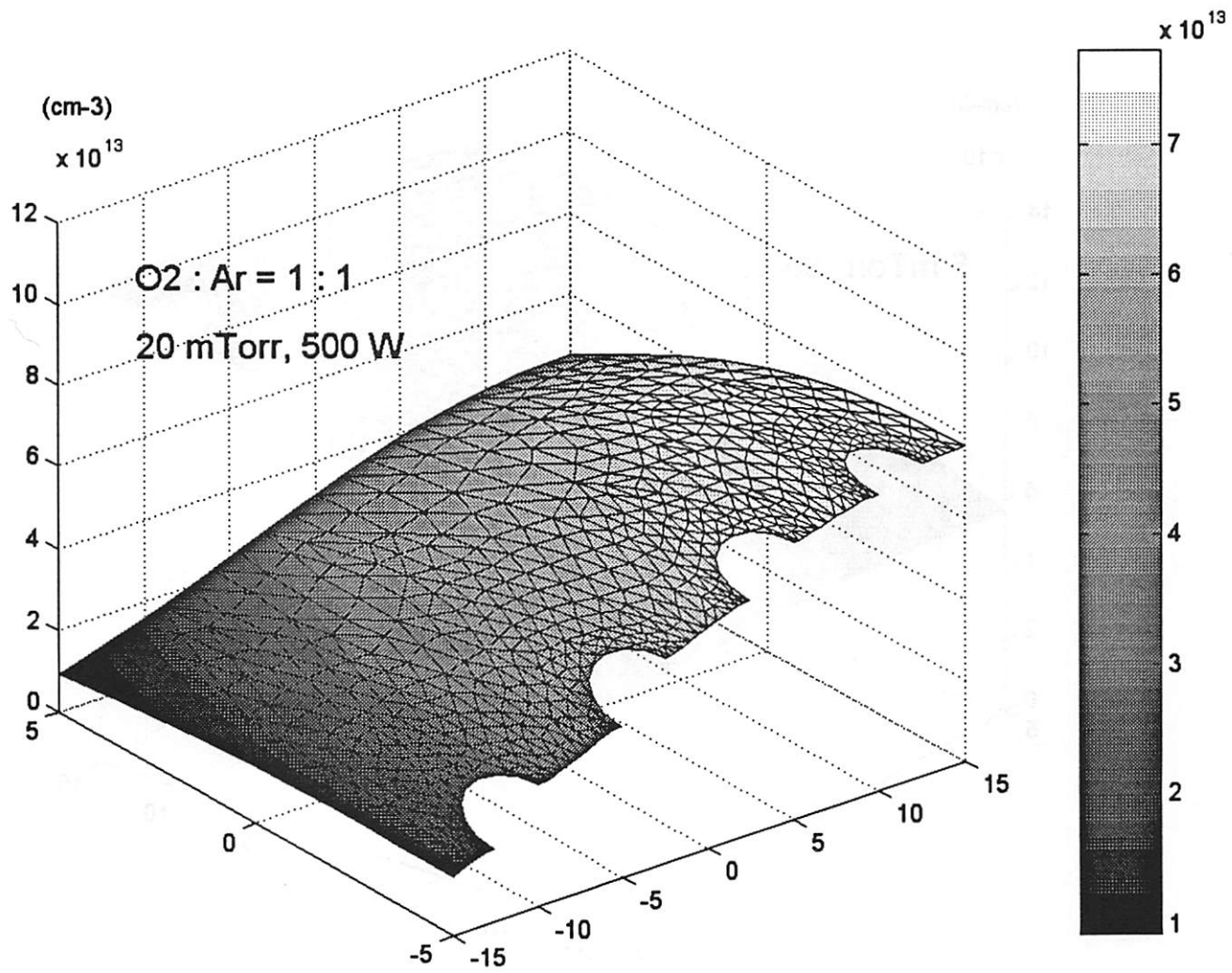


Fig. 7(b). O-atom density profile for an O<sub>2</sub>/Ar mixture discharge at 20 mTorr.

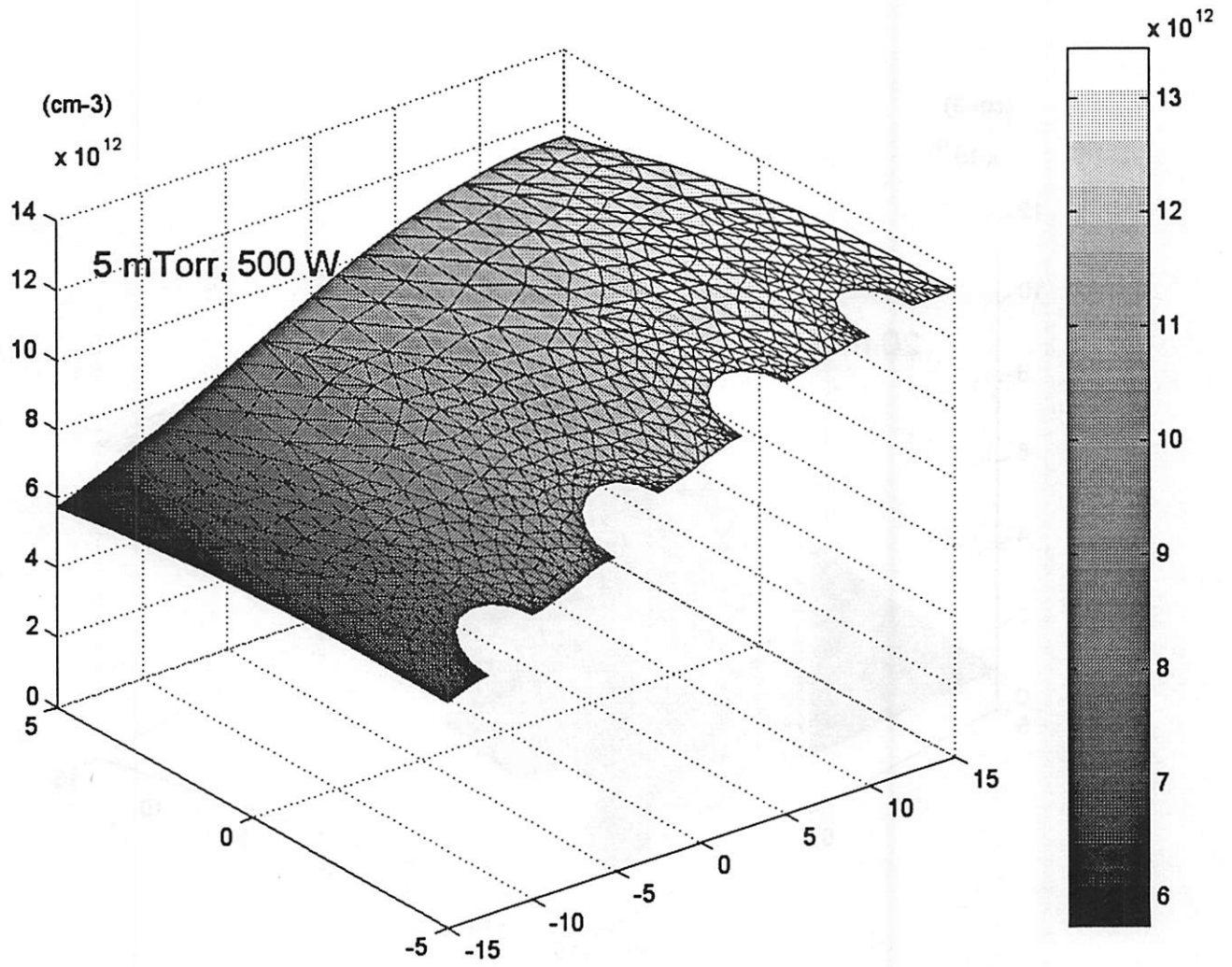


Fig. 8(a). O-atom density profile for a pure O<sub>2</sub> discharge at 5 mTorr.

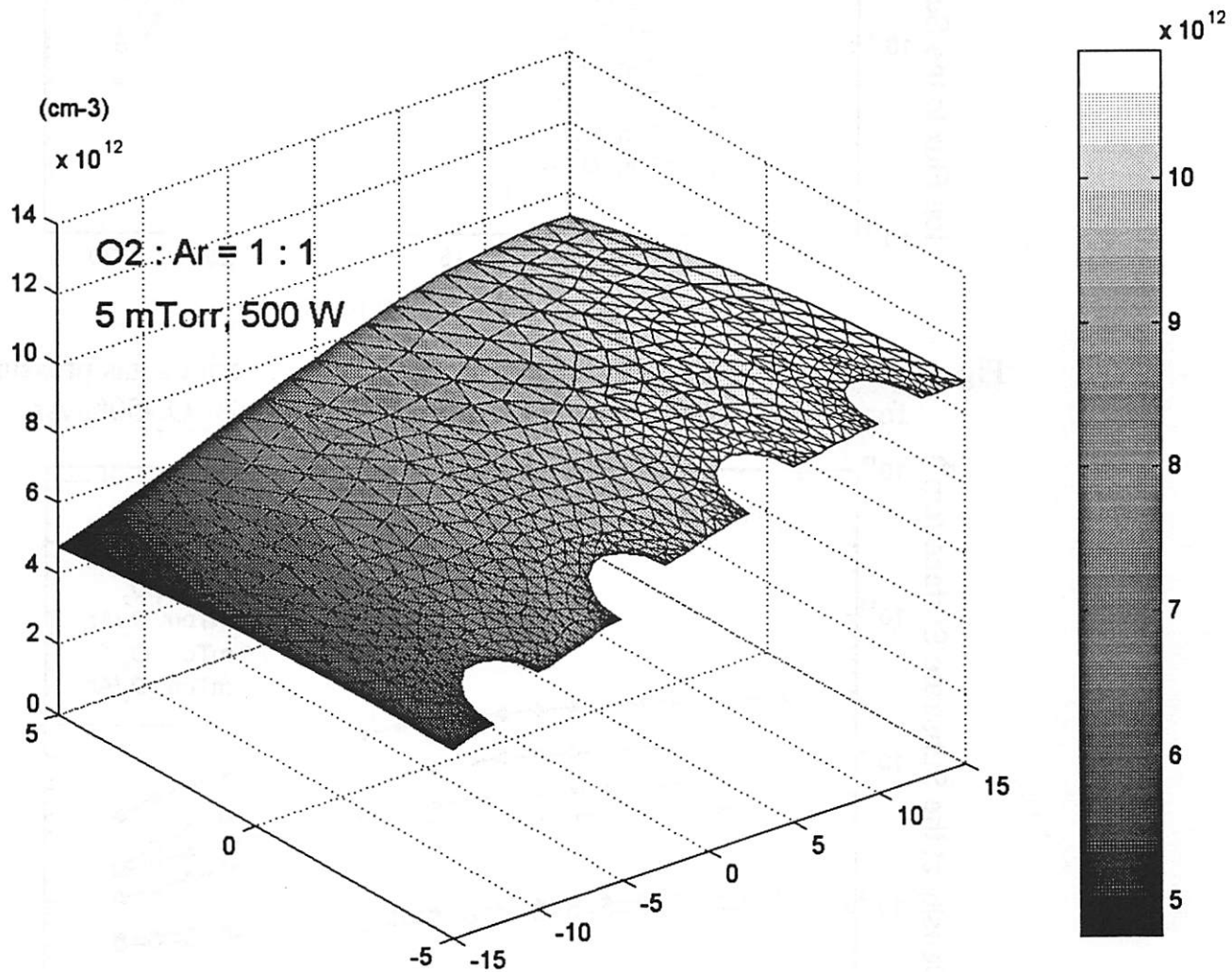


Fig. 8(b). O-atom density profile for an O<sub>2</sub>/Ar mixture discharge at 5 mTorr.

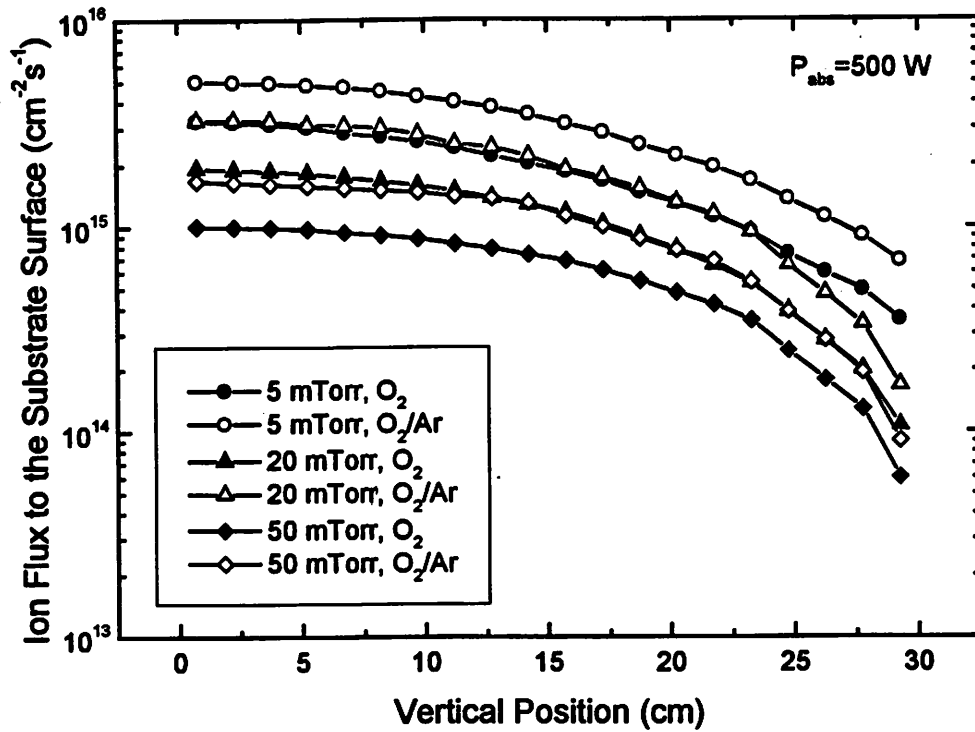


Fig. 9. Computed ion flux to the substrate surface at various gas pressures for a pure  $O_2$  plasma and  $O_2/Ar$  mixture with 50%  $O_2$ -50% Ar.

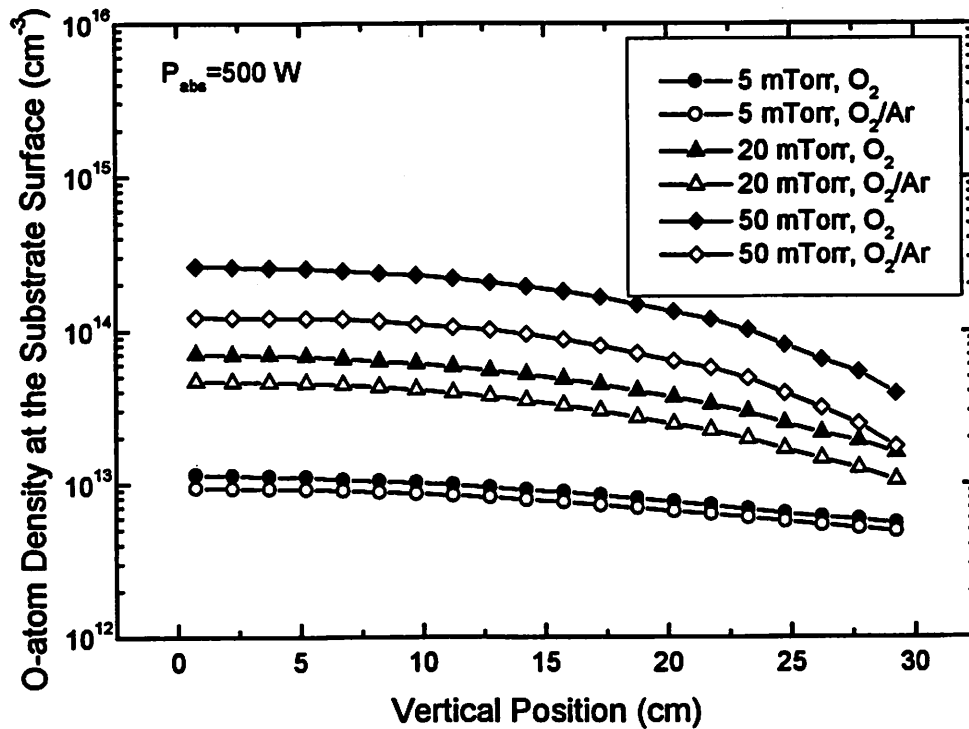


Fig. 10. Computed O-atom density at the substrate surface at various gas pressures for a pure  $O_2$  plasma and  $O_2/Ar$  mixture with 50%  $O_2$ -50% Ar.

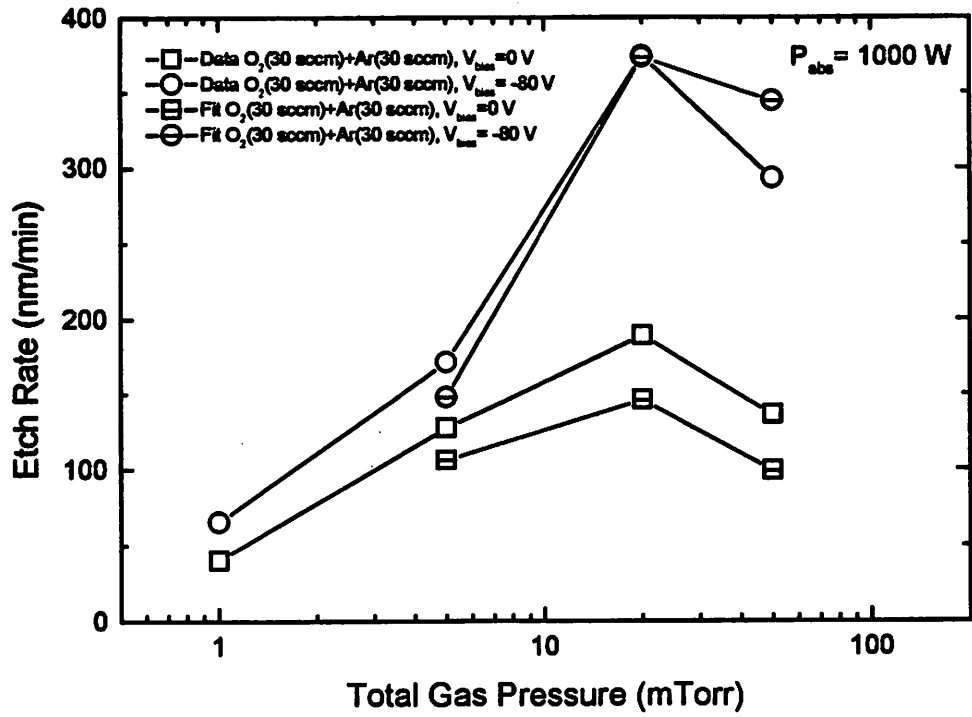


Fig. 11. Plots of etch rate vs total gas pressure. The fits are from Eq. (13) with the simulation results in Figs. 9 and 10.